

All-Donor Poly(arylene-ethynylene)s Containing Anthracene and Silole-Based Units: Synthesis, Electronic, and Photovoltaic Properties

Roberto Grisorio,¹ Gian Paolo Suranna,¹ Piero Mastrorilli,^{1,2} Giovanni Allegretta,³ Anna Loiudice,^{4,5} Aurora Rizzo,^{5,6} Giuseppe Gigli,^{4,5,6} Kyriaki Manoli,³ Maria Magliulo,³ Luisa Torsi³

¹DICATECh: Dipartimento di Ingegneria Civile, Ambientale, del Territorio, Edile e di Chimica, Polytechnic of Bari, Campus Universitario, via Orabona 4, 70125 Bari, Italy

²Consiglio Nazionale delle Ricerche, Istituto di Chimica dei Composti Organometallici (ICCOM-CNR), via Orabona 4, 70125 Bari, Italy

³Università degli Studi "Aldo Moro" di Bari, Dipartimento di Chimica, via Orabona 4, 70126 Bari, Italy

⁴Dipartimento di Matematica e Fisica "E. De Giorgi", Università del Salento, via Monteroni, 73100 Lecce, Italy

⁵CBN - Center for Biomolecular Nanotechnologies, Italian Institute of Technology - Energy Platform, via Barsanti sn-73010, Arnesano (LE), Italy

⁶NNL CNR-Istituto Nanoscienze, c/o Distretto Tecnologico, via per Arnesano km 5, 73100 Lecce, Italy

Correspondence to: G. P. Suranna (E-mail: surannag@poliba.it)

Received 4 July 2013; accepted 15 August 2013; published online 18 September 2013

DOI: 10.1002/pola.26914

ABSTRACT: The manuscript deals with the synthesis and properties of four new all-donor alternating poly(arylene-ethynylene)s **DBSA**, **DBSTA**, **DTSA**, and **DTSTA**. The polymers have been obtained by a Sonogashira cross-coupling of 9,10-diethynyl-anthracene with the dibromo-derivatives of 9,9-dioctyl-dibenzosilole (**DBSA**), 2,7-dithienyl-9,9-dioctyl-dibenzosilole (**DBSTA**), 4,4-dioctyl-dithienosilole (**DTSA**), or 2,6-dithienyl-9,9-dioctyl-dithienosilole (**DTSTA**). The polymers exhibited absorption profiles and frontier orbital energies strongly dependent on their primary structure. Density functional theory calculations confirmed experimental observations and provided an insight into the electronic structure of the macromolecules. In particular, the effects exerted by the thiophene units in **DBSTA** and **DTSTA** on the optical properties of the corresponding

polymers could be rationalized with respect to **DBSA** and **DTSA**. Preliminary photovoltaic measurements have established that the performance of **DTSA** is among the highest reported for an all-donor polymer. Moreover, UV irradiation of **DTSA** films under air evidenced a remarkable photostability of this material, providing further evidence that ethynylene-containing electron-rich systems are promising donors for organic solar cells applications. © 2013 Wiley Periodicals, Inc. *J. Polym. Sci., Part A: Polym. Chem.* **2013**, *51*, 4860–4872

KEYWORDS: anthracene; bulk hetero-junction solar cells; conjugated polymers; dibenzosilole; dithienosilole; light harvesting donors; photophysics; polyaromatics; poly(arylene-ethynylene)s

INTRODUCTION The π -conjugated polymers have widely been employed as light-harvesting electron donor materials in bulk heterojunction (BHJ) solar cells, since they can be suitably designed to provide the necessary light harvesting as well as a favorable mixing with fullerene-based electron acceptors.¹ An ideal donor material for BHJ solar cells should possess the following requisites: (i) a broad absorption spectrum in the range of wavelengths where the solar photon flux is maximum (i.e., 500–800 nm); (ii) a thermodynamically feasible electron transfer to the acceptor materials (usually fullerene derivatives); (iii) an efficient hole transport; (iv) a relatively deep highest occupied molecular orbital (HOMO) energy. All these properties independently influence

the figures of merit of the photovoltaic devices, namely the short circuit current (J_{sc}), the fill factor (FF), and the open circuit voltage (V_{oc}).²

In particular, in order to maximize the light harvesting properties of the active layer, the obtainment of conjugated materials with suitably low band-gap is crucial. The band-gap engineering of a conjugated material is extremely important to enhance the solar cell photocurrent, since the amount of absorbed light depends both on the absorption wavelength and on its extinction coefficient. From the chemical point of view, the donor-acceptor approach³ has proved remarkably effective for the synthetic design of narrow band-gap

Additional Supporting Information may be found in the online version of this article.

© 2013 Wiley Periodicals, Inc.

π -conjugated macromolecules. On the other hand, their wider band-gap all-donor counterparts, with the exception of regio-regular poly(3-hexyl)thiophene (P3HT),⁴ did not thus far exhibit impressive performances in BHJ applications. In donor-acceptor materials, the band-gap contraction is the result of an intramolecular charge transfer from the electron-rich to the electron-poor unit. Furthermore, the presence of electron poor units in a π -conjugated backbone could bring advantages in terms of V_{OC} , lowering the HOMO energy of the corresponding polymer. However, some features of the donor-acceptor concept can result detrimental for the BHJ performances, since the electron-withdrawing units might impair the hole transport within the active layer of the BHJ solar cell and, concentrating the electron density at the excited state, inhibit the electron transfer to the fullerene.⁵

Aiming at the obtainment of low band-gap semiconductors, the choice of the appropriate class of polymers is the first step. In poly(arylene-ethynylene)s,⁶ the presence of the ethynylene bridges can attenuate some steric and conformational constraints, favoring the achievement of relatively planar structures with a consequent band gap lowering. Anthracene is a smaller acene that, due to its higher stability with respect to tetracene and pentacene is receiving a growing attention as building block for its manifold applications in organic electronics.⁷ The combination between the rigid electron-rich anthracene core and the ethynylene bridges give rise to the 9,10-diethynyl-anthracene unit, which not only promotes the planarization of the polymeric backbone, but also favors strong intermolecular π - π stacking with prospected beneficial influence on the hole transport.⁸ Moreover, flanking another electron-rich moiety to the anthracene can lead to the fine tuning of the absorption properties, frontier orbital energies, and hole transport of the corresponding material. It has been shown how the incorporation of 9,10-diethynyl-anthracene units into a poly(*p*-phenylene-vinylene) backbone could lead to good hole carrier mobilities and power conversion efficiencies of up to 3.8%.⁹ However, a strategy based on the mere construction of a π -conjugated material made of all-donor units could bring to an increase of the HOMO energy, negatively affecting the V_{OC} of the corresponding solar cell. It is therefore advisable to properly choose the further donor unit flanking the anthracene unit, in order to avoid the aforementioned drawback, and in this respect, silacyclopentadiene-based materials are gaining considerable attention. Silacyclopentadiene (silole) is endowed with a low lowest unoccupied molecular orbital (LUMO) energy as a consequence of the interaction between the σ^* orbital of the silylene moiety, effectively interacting with the π^* orbital of the butadiene fragment.¹⁰ As a result, the low band gap of silole-containing materials does not occur at the expenses of the increase in HOMO level, thereby preserving a condition for a sufficiently high V_{OC} . It is therefore not surprising that dithienosilole and dibenzosilole building blocks are being especially employed for the preparation of host material for BHJ solar cells.¹¹ Part of this interest is due to the fact that the higher C-Si bond distance (~ 0.3 Å) within the polymer backbone allows for better interchain packing

and improved hole mobility. Moreover, the possible functionalization of the silicon atom with two alkyl chains adds a degree of freedom to the solubility and processability of the corresponding polymers and allows a further control of the intermolecular polymer/fullerene interactions, aimed at favoring the formation of a suitable interpenetrating network in the BHJ active layer.

Having previously studied anthracene-based oligomers and polymers for both field-effect transistor and organic photovoltaics applications,¹² we have decided to synthesize alternating poly(arylene-ethynylene)s containing 9,10-diethynyl-anthracene and suitably functionalized dithienosilole (**DTSA**) or dibenzosilole (**DBSA**) repeating units. The properties of these materials were compared with those of the corresponding polymers containing dithienyl-dithienosilole and dithienyl-dibenzosilole (**DTSTA** and **DBSTA**, respectively) units that were synthesized aiming at improving optical response and hole mobility. While better hole mobilities were obtained with **DBSTA** in field effect transistors, the best power conversion efficiencies (1.5%, among the highest for all-donor macromolecules in BHJ solar cells) were achieved using **DTSA** in blend with PC₆₁BM.

EXPERIMENTAL

General Remarks

9,10-Diethynylanthracene,¹³ 3,7-dibromo-5,5-di-*n*-octyl-dibenzo [b,d]silole¹⁴ (**1**), 3,3'-dibromo-2,2'-bithiophene (**4**),¹⁴ and Pd(PPh₃)₄¹⁵ were synthesized according to literature procedures, while the other reactants were purchased from standard commercial sources and used as received. All solvents used were carefully dried and freshly distilled according to standard laboratory practice. All manipulations were carried out under inert nitrogen atmosphere. Flash chromatography was performed using a silica gel of 230–400 mesh. ¹H and ¹³C{¹H} NMR spectra were recorded on a Bruker Avance 700 MHz instrument. The purity of all title compounds was judged to be > 95 % as determined by a combination of ¹H and ¹³C NMR analyses. FTIR measurements were carried out on a JASCO FTIR 4200 spectrophotometer. UV-vis spectra were recorded on a Jasco V-670 instrument. Photoluminescence (PL) spectra were obtained on a Varian Cary Eclipse spectrophotometer. Gel permeation chromatography (GPC) analyses were carried out on an Agilent Series 1100 instrument equipped with a PL-gel 5 μ m mixed-C column. THF solutions for GPC analysis were eluted at 25 °C at a flow rate of 1.0 mL min⁻¹ and analyzed using a multiple wave UV-vis detector. Number average molecular weights (M_n), weight average molecular weights (M_w) and polydispersity index (PDI) are relative to polystyrene standards. Thermogravimetric analyses (TGA) were performed under a nitrogen atmosphere (flow of 40 mL min⁻¹) with a Perkin-Elmer Pyris 6 TGA in the range from 30 to 800 °C with a heating rate of 10 °C min⁻¹. Melting points were measured on a Büchi B-545 instrument. Elemental analyses were obtained on a EuroVector CHNS EA3000 instrument. Cyclic voltammetry (CV) was carried out on a Metrohm Autolab PGSTAT 302-N potentiostat. The materials were drop cast on a glassy carbon-

working electrode from a 1 mg mL⁻¹ chloroform solution. Measurements were carried at 25 °C in acetonitrile solution containing tetrabutylammonium tetrafluoroborate (0.025 M) as supporting electrolyte with a scan rate of 25 mV s⁻¹. The potentials were measured versus Ag/Ag⁺ as the quasi-reference electrode. After each experiment, the potential of the Ag/Ag⁺ electrode was calibrated against the ferrocene/ferrocenium (Fc/Fc⁺) redox couple. The electrochemical energy gap was determined as the difference between the onsets of the oxidation and reduction potentials ($E_g^{\text{elc}} = E_{\text{ox}}^{\text{onset}} - E_{\text{red}}^{\text{onset}}$). The HOMO and LUMO energy values were estimated from the onset potentials of the first oxidation and reduction event, respectively. After calibration of the measurements against Fc/Fc⁺, the HOMO and LUMO energy levels were calculated according to the following equations:

$$E_{\text{HOMO}} (\text{eV}) = -[E_{\text{ox}}^{\text{onset}} - E_{1/2}(\text{Fc}/\text{Fc}^+) + 4.8]$$

$$E_{\text{LUMO}} (\text{eV}) = -[E_{\text{red}}^{\text{onset}} - E_{1/2}(\text{Fc}/\text{Fc}^+) + 4.8]$$

where $E_{1/2}(\text{Fc}/\text{Fc}^+)$ is the half-wave potential of the Fc/Fc⁺ couple (the oxidation potential of which is assumed at +4.8 eV below the vacuum level) against the Ag/Ag⁺ electrode. Analyses of the ground-state structures for the molecules were carried out using the density functional theory (DFT). The B3LYP functional was used in conjunction with the 6-31G(d,p) or 3-21G(d) basis set. Time-dependent DFT (TDDFT) calculations were performed to assess the excited-state transition energies. All calculations were carried out with the Gaussian09 program¹⁶ package and performed on isolated molecules *in vacuo*. UV-photodecomposition experiments (>300 nm) were carried out by irradiating the sample with a 150-W high-pressure Hg lamp for 2 h. The samples were placed at 1 cm from the UV source.

Device Construction

The synthesized polymers were tested in BHJ solar cells with structure ITO/poly(3,4-ethylenedioxythiophene):poly(styrenesulfonate) (PEDOT:PSS)/polymer:PC₆₁BM/LiF/Al. The photovoltaic devices were fabricated on patterned ITO-coated glass substrates as the anode. ITO glass substrates were sequentially cleaned by ultrasonication in deionized water, acetone, isopropyl alcohol, and cleaned for 10 min in a TL-1 solution at 85 °C. The ITO surface was then modified by spin-coating of a conductive PEDOT:PSS thin film (40 nm) purchased by HC Starck, followed by a baking at 140 °C in nitrogen atmosphere for 15 min. Subsequently, the active layer blend (~100 nm) was deposited by spin coating a chloroform solution of the relevant compound and [6,6]-phenyl-C₆₁-butyric acid methyl ester (PC₆₁BM, Nano-C) at 700 rpm for 240 s. All the operations concerning the deposition of the active layer were performed in a glove box under a nitrogen atmosphere. The LiF (0.6 nm) and Al (150 nm) electrodes were thermally evaporated at low pressure (<7 × 10⁻⁶ Torr) through a shadow mask. The active area of each device (~0.04 cm²) was accurately determined by an optical microscope equipped with a ruler. The device measurements were carried out in ambient conditions under illu-

mination of one-sun (AM 1.5G). The atomic force microscopy (AFM) topography images were acquired with a XE-100 PSIA Park Scanning Probe Microscope in noncontact mode.

Organic thin-film transistor devices were fabricated in top-contact configurations using a highly *n*-doped silicon wafer (resistivity: 20 Ω cm) as a gate electrode on which 300 nm of dielectric (SiO₂) was thermally grown. After suitable surface cleaning, films of the relevant polymers were deposited by spin-coating from 2.0 mg mL⁻¹ chloroform solutions. Drain and source electrodes were fabricated on the organic semiconducting layer by thermal evaporation through a shadow mask. The devices were measured with an Agilent 4155 C semiconductor parameter analyzer in ambient conditions. The field-effect mobility (μ) and threshold voltage (V_{th}) were extracted from the relevant (I_{DS})^{1/2} versus gate voltage (V_g) plot in the saturation regime obtained from the device transfer characteristics.

3,7-Di(thiophen-2-yl)-5,5-di-*n*-octyl-dibenzo[*b,d*]silole (2)

A mixture of **1** (0.60 g, 1.06 mmol), *n*-tributyl(thiophen-2-yl)stannane (0.89 g, 2.35 mmol), and Pd(PPh₃)₄ (70 mg, 0.06 mmol) in toluene (10 mL) was refluxed for 24 h under vigorous stirring. The mixture was cooled to room temperature, diluted with chloroform (100 mL), washed with water (3 × 50 mL) and dried over Na₂SO₄. After solvent removal, the crude product was purified by column chromatography (SiO₂, petroleum ether 40–60 °C:dichloromethane = 9:1) to yield **2** (0.55 g, 91%) as an off-white solid.

M.p. = 76.9–77.9 °C. ¹H NMR (CDCl₃): δ 7.89 (d, *J* = 1.5 Hz, 2H), 7.83 (d, *J* = 7.9 Hz, 2H), 7.71 (dd, *J* = 7.9, 1.5 Hz, 2H), 7.39 (d, *J* = 3.7 Hz, 2H), 7.32 (d, *J* = 5.0 Hz, 2H), 7.13 (dd, *J* = 5.0, 3.7 Hz, 2H), 1.45–1.40 (m, 4H), 1.33–1.19 (m, 20H), 1.05–1.01 (m, 4H), 0.86 (t, *J* = 7.0 Hz, 6H) ppm; ¹³C{¹H} NMR (CDCl₃): δ 147.3, 144.7, 138.9, 133.2, 130.6, 128.0, 127.9, 124.6, 122.9, 121.3, 33.3, 31.8, 29.2, 29.1, 23.9, 22.6, 14.0, 12.3 ppm. ELEM. ANAL. Calcd for C₃₆H₄₆S₂Si: C, 75.73; H, 8.12. Found: C, 75.71; H, 8.10.

3,7-Bis(2-bromothiophen-5-yl)-5,5-di-*n*-octyl-dibenzo[*b,d*]silole (3)

N-Bromosuccinimide (NBS; 0.25 g, 1.43 mmol) was slowly added to a solution of **2** (0.40 g, 0.70 mmol) in DMF (15 mL) at room temperature and the obtained mixture was stirred overnight. The reaction mixture was poured into water (100 mL) and the formed precipitate was collected by filtration. The crude product was then purified by column chromatography (SiO₂, petroleum ether 40–60 °C) to afford **3** (0.43 g, 85%) as a pale yellow solid.

M.p. = 84.0–85.0 °C. ¹H NMR (CDCl₃): δ 7.91 (d, *J* = 1.5 Hz, 2H), 7.82 (d, *J* = 7.9 Hz, 2H), 7.69 (dd, *J* = 7.9, 1.5 Hz, 2H), 7.49 (d, *J* = 4.8 Hz, 2H), 7.23 (d, *J* = 4.8 Hz, 2H), 1.45–1.40 (m, 4H), 1.33–1.19 (m, 20H), 1.05–1.01 (m, 4H), 0.86 (t, *J* = 7.0 Hz, 6H) ppm. ¹³C{¹H} NMR (CDCl₃): δ 143.9, 140.8, 134.8, 132.4, 132.2, 131.1, 129.3, 129.1, 128.0, 127.6, 33.2, 31.9, 29.2, 29.1, 23.8, 22.5, 14.0, 12.2 ppm. ELEM. ANAL. Calcd for C₃₆H₄₄Br₂S₂Si: C, 59.33; H, 6.09. Found: C, 59.35; H, 6.10.

4,4-Di-*n*-octyl-silolo[3,2-*b*:4,5-*b'*]dithiophene (**5**)

A mixture of **4** (9.72 g, 30.00 mmol) in anhydrous THF (50 mL) was added dropwise to a *n*-BuLi solution (1.6 M in hexanes, 24.0 mL, 60.00 mmol) in THF (50 mL) kept at $-78\text{ }^{\circ}\text{C}$ under a vigorous stirring. After 1 h reaction at $-78\text{ }^{\circ}\text{C}$, the formation of a white suspension was observed. Subsequently, a solution of di-*n*-octyl-dichlorosilane (8.07 g, 30.00 mmol) in THF (100 mL) was added dropwise. The mixture was stirred for further 5 h at $-78\text{ }^{\circ}\text{C}$, then allowed to reach room temperature. After overnight stirring, the reaction was quenched by adding a saturated aqueous NH_4Cl solution (300 mL). The aqueous layer was extracted with diethyl ether ($3 \times 100\text{ mL}$). The organic phases were then combined, washed with water and dried over MgSO_4 . After solvent removal, the crude product was purified by column chromatography (SiO_2 , petroleum ether $40\text{--}60\text{ }^{\circ}\text{C}$) to give **5** (6.80 g, 68% yield) as a greenish oil.

^1H NMR (CDCl_3): δ 7.21 (d, $J = 4.6\text{ Hz}$, 2H), 7.07 (d, $J = 4.6\text{ Hz}$, 2H), 1.43–1.37 (m, 4H), 1.33–1.21 (m, 20H), 0.94–0.88 (m, 10H) ppm. $^{13}\text{C}\{^1\text{H}\}$ NMR (CDCl_3): δ 149.2, 141.6, 129.6, 125.0, 33.2, 31.9, 29.2, 29.1, 24.2, 22.7, 14.1, 11.9 ppm.

2,6-Dibromo-4,4-di-*n*-octyl-silolo[3,2-*b*:4,5-*b'*]dithiophene (**6**)

NBS (1.98 g, 11.00 mmol) was added portionwise to a solution of **5** (2.25 g, 5.38 mmol) in DMF (40 mL) at room temperature. The mixture was stirred for 10 min before the addition of water (50 mL). Subsequently, the compound was extracted with diethyl ether ($3 \times 50\text{ mL}$) and the combined organic phases were dried over Na_2SO_4 . After solvent removal, the crude product was purified by column chromatography (SiO_2 , petroleum ether $40\text{--}60\text{ }^{\circ}\text{C}$) to afford **6** (2.82 g, 91%) as a greenish oil.

^1H NMR (CDCl_3): δ 7.01 (s, 2H), 1.38–1.32 (m, 4H), 1.31–1.20 (m, 20H), 0.91–0.87 (m, 10H) ppm. $^{13}\text{C}\{^1\text{H}\}$ NMR (CDCl_3): δ 148.9, 141.1, 132.2, 111.4, 33.1, 31.8, 29.2, 29.1, 24.0, 22.6, 14.1, 11.6 ppm.

2,6-Di(thiophen-2-yl)-4,4-di-*n*-octyl-silolo[3,2-*b*:4,5-*b'*]dithiophene (**7**)

A mixture of **6** (0.56 g, 0.97 mmol), tri-*n*-butyl(thiophen-2-yl)stannane (0.71 g, 1.94 mmol), and $\text{Pd}(\text{PPh}_3)_4$ (112 mg, $0.97 \times 10^{-1}\text{ mmol}$) in toluene (20 mL) was refluxed for 24 h under vigorous stirring. Upon cooling down the reaction to room temperature, the mixture was diluted with dichloromethane and washed with water, and the obtained organic phase was dried over Na_2SO_4 . After solvent removal, the crude product was purified by column chromatography (SiO_2 , petroleum ether $40\text{--}60\text{ }^{\circ}\text{C}$) to give **7** (0.46 g, 82%) as an orange oil.

^1H NMR (CDCl_3): δ 7.21 (dd, $J = 4.9, 1.0\text{ Hz}$, 2H), 7.18 (dd, $J = 3.6, 1.0\text{ Hz}$, 2H), 7.14 (s, 2H), 7.04 (dd, $J = 4.9, 3.6\text{ Hz}$, 2H), 1.39–1.33 (m, 4H), 1.31–1.20 (m, 20H), 0.92–0.87 (m, 10H) ppm. $^{13}\text{C}\{^1\text{H}\}$ NMR (CDCl_3): δ 147.7, 142.9, 138.1, 137.7, 127.8, 126.4, 123.9, 123.3, 33.2, 31.8, 29.1, 29.0, 24.1, 22.6, 14.1, 11.8 ppm.

2,6-Bis(5-bromothiophen-2-yl)-4,4-di-*n*-octyl-silolo[3,2-*b*:4,5-*b'*]dithiophene (**8**)

NBS (0.30 g, 1.66 mmol) was added portionwise to a solution of **7** (0.40 g, 0.83 mmol) in DMF (20 mL) at room temperature and the obtained mixture stirred overnight. The reaction was quenched with water (50 mL) and extracted ($3 \times 50\text{ mL}$) with diethyl ether. The combined organic phases were dried over Na_2SO_4 . After solvent removal, the crude product was purified by column chromatography (SiO_2 , petroleum ether $40\text{--}60\text{ }^{\circ}\text{C}$) to afford **8** (0.50 g, 81%) as an orange oil.

^1H NMR (CDCl_3): δ 7.46 (d, $J = 4.5\text{ Hz}$, 2H), 7.24 (s, 2H), 7.20 (d, $J = 4.5\text{ Hz}$, 2H), 1.32–1.22 (m, 24H), 0.88–0.86 (m, 10H) ppm. $^{13}\text{C}\{^1\text{H}\}$ NMR (CDCl_3): δ 146.8, 145.9, 139.3, 137.5, 127.5, 126.2, 124.9, 123.4, 33.3, 31.9, 29.1, 28.9, 24.2, 22.6, 14.1, 11.8 ppm.

Poly(9,9-di-*n*-octyl-dibenzosilole-2,7-diyl-ethynylene-anthracen-9,10-diyl-ethynylene) (DBSA)

A mixture of **1** (0.29 g, 0.51 mmol), 9,10-diethynylanthracene (0.12 g, 0.51 mmol), $\text{Pd}(\text{PPh}_3)_4$ (59 mg, $5.4 \times 10^{-2}\text{ mmol}$), CuI (10 mg, $5.0 \times 10^{-2}\text{ mmol}$), triethylamine (10 mL), and toluene (10 mL) was stirred at $90\text{ }^{\circ}\text{C}$ for 15 min. The reaction mixture was cooled to room temperature, diluted with chloroform, and washed with water. After solvent removal, the crude product was dissolved into the minimum amount of chloroform and precipitated twice with methanol. The collected powder was washed in a Soxhlet apparatus using methanol and acetone, then dissolved in chloroform. The volume of the chloroform fraction was reduced before precipitation with methanol. The obtained solid was filtered and eventually dried under vacuum overnight to afford **DBSA** (51% yield) as a red powder.

^1H NMR (CDCl_3): δ 8.79–7.58 (m, 14H), 1.42–1.24 (m, 24H), 1.10–1.01 (m, 4H), 0.92–0.85 (m, 6H) ppm. ELEM. ANAL. Calcd for $(\text{C}_{46}\text{H}_{48}\text{Si})_n$: C, 87.84; H, 7.69. Found: C, 86.76; H, 7.37. IR (KBr): ν 3058, 2954, 2919, 2879, 2184, 1456, 1403, 762 cm^{-1} . GPC: $M_n = 16,200\text{ Da}$; PDI = 2.0.

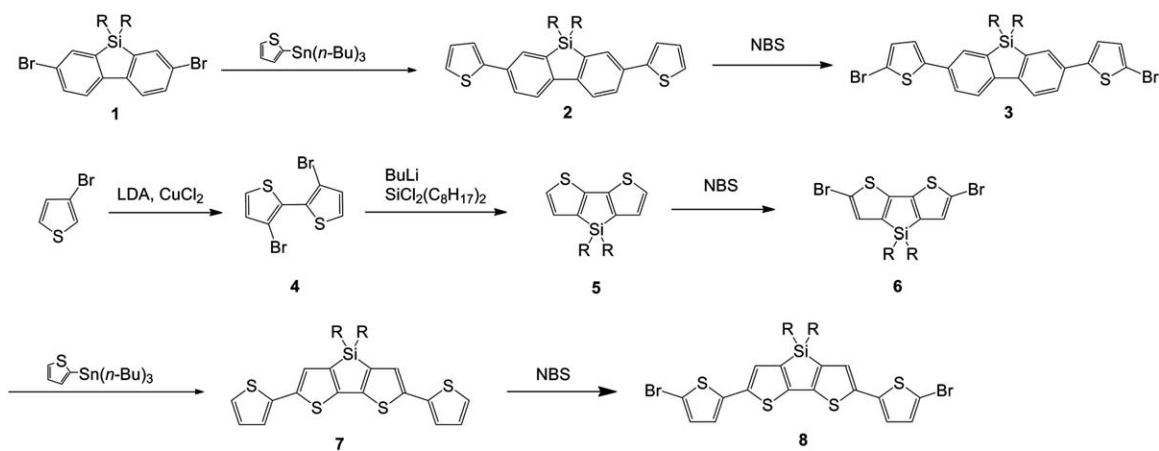
Poly[2,7-di(thiophen-2-yl)-9,9-di-*n*-octyl-dibenzosilole-5',5''-diyl-ethynylene-anthracen-9,10-diyl-ethynylene] (DBSTA)

Following the procedure reported for **DBSA**, the polymer **DBSTA** was obtained by reacting **3** (0.91 g, 1.24 mmol), 9,10-diethynylanthracene (0.28 g, 1.24 mmol), $\text{Pd}(\text{PPh}_3)_4$ (63 mg, $5.4 \times 10^{-2}\text{ mmol}$), CuI (10 mg, $5.4 \times 10^{-2}\text{ mmol}$), triethylamine (15 mL), and toluene (15 mL). The material was obtained as a deep red solid (48% yield).

^1H NMR (CDCl_3): δ 8.87–7.61 (m, 18H), 1.43–1.21 (m, 24H), 1.12–1.00 (m, 4H), 0.94–0.85 (m, 6H) ppm. ELEM. ANAL. Calcd for $(\text{C}_{54}\text{H}_{52}\text{S}_2\text{Si})_n$: C, 81.77; H, 6.61. Found: C, 81.06; H, 5.99. IR (KBr): ν 3058, 2954, 2919, 2879, 2185, 1455, 1403, 763 cm^{-1} . GPC: $M_n = 7400\text{ Da}$; PDI = 1.3.

Poly[4,4-di-*n*-octyl-dithienosilole-2,6-diyl-ethynylene-anthracen-9,10-diyl-ethynylene] (DTSA)

Following the procedure reported for **DBSA**, the polymer **DTSA** was obtained by reacting **6** (0.29 g, 0.50 mmol), 9,10-



SCHEME 1 Synthesis of monomers **3**, **6**, and **8** ($R = n$ -octyl).

diethynylantracene (0.11 g, 0.50 mmol), $\text{Pd}(\text{PPh}_3)_4$ (58 mg, 5.0×10^{-2} mmol), CuI (10 mg, 5.0×10^{-2} mmol), triethylamine (15 mL), and toluene (15 mL). The material was isolated as a deep violet solid (65% yield).

^1H NMR (CDCl_3): δ 8.82–7.39 (m, 10H), 1.34–1.21 (m, 24H), 0.89–0.85 (m, 10H) ppm. ELEM. ANAL. Calcd for $(\text{C}_{42}\text{H}_{44}\text{S}_2\text{Si})_n$: C, 78.70; H, 6.92. Found: C, 78.16; H, 6.87. IR (KBr): ν 3058, 2954, 2920, 2878, 2166, 1349, 1167, 759 cm^{-1} . GPC: $M_n = 10,800$ Da; PDI = 1.8.

Poly[4,4-di-*n*-octyl-2,6-di(thiophen-2-yl)-dithienosilole-5',5''-diyl-ethynylene-anthracen-9,10-diyl-ethynylene] (DTSTA)

Following the procedure reported for **DBSA**, the polymer **DTSTA** was obtained by reacting **8** (0.11 g, 0.15 mmol), 9,10-diethynylantracene (34 mg, 0.15 mmol), $\text{Pd}(\text{PPh}_3)_4$ (17 mg, 1.5×10^{-2} mmol), CuI (3 mg, 1.5×10^{-2} mmol), triethylamine (3 mL), and toluene (3 mL). The material was isolated as a deep red solid (57% yield).

^1H NMR (CDCl_3): δ 8.82–7.49 (m, 14H) ppm, 1.34–1.21 (m, 24H), 0.89–0.85 (m, 10H) ppm. ELEM. ANAL. Calcd for $(\text{C}_{50}\text{H}_{48}\text{S}_4\text{Si})_n$: C, 74.58; H, 6.01. Found: C 74.16; H 5.87. IR (KBr): ν 3058, 2954, 2919, 2879, 2167, 1348, 1166, 760 cm^{-1} . GPC: $M_n = 5600$ Da; PDI = 1.4.

RESULTS AND DISCUSSION

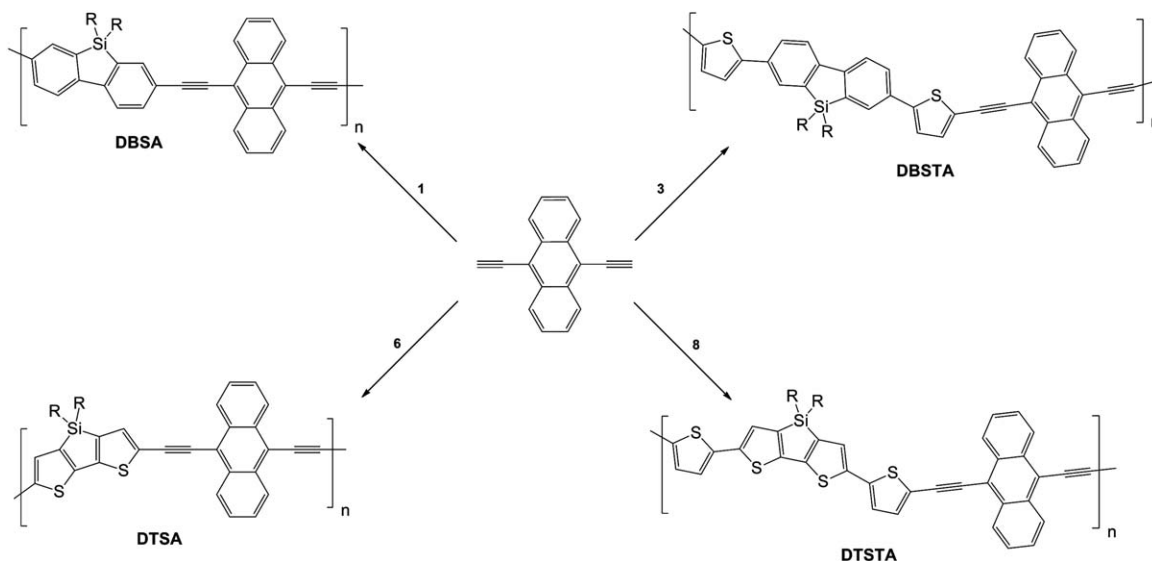
Polymers Preparation and Characterization

The synthetic approach for the obtainment of the silole-based monomers is described in Scheme 1. The preparation of 2,7-dithienyl-9,9-di-*n*-octyl-dibenzosilole (**2**) was achieved by a $\text{Pd}(\text{PPh}_3)_4$ -catalyzed Stille cross-coupling of 2,7-dibromo-9,9-di-*n*-octyl-dibenzosilole (**1**) with tri-*n*-butyl(thiophen-2-yl)stannane. The obtained product was submitted to a bromination with NBS to afford the corresponding dibromo-derivative (**3**), to be used in the polymerization reaction. For the preparation of dithienosilole monomers, the commercially available 3-bromothiophene was reacted with lithium diisopropylamide in THF at -80 °C. After metalation,

CuCl_2 was added to promote the formation of the corresponding homo-coupling product 3,3'-dibromo-2,2'-bithiophene (**4**). The subsequent step consisted in the formation of the silole ring, that was obtained by treating **4** with *n*-butyl lithium (BuLi) at -80 °C, followed by the addition of the di(*n*-octyl)dichloro-silane, that afforded the dithienosilole derivative **5** in good yield (68%). The corresponding dibromo-derivative **6**, to be used in the polymerization reactions, was obtained in 91% yield by bromination of **5** with NBS. The introduction of the thiophene units was carried out by using $\text{Pd}(\text{PPh}_3)_4$ -catalyzed Stille reaction between **6** and tri-*n*-butyl(thiophen-2-yl)stannane to obtain the dithienyl-derivative **7** in 82% yield. The reaction of **7** with NBS gave the corresponding dibromo-derivative **8** in 81% yield.

The synthetic sequence for the obtainment of the polymers is reported in Scheme 2. All materials were prepared by a Pd-catalyzed Sonogashira coupling between the silole-based monomers **1**, **3**, **6**, and **8** and an equivalent amount of 9,10-diethynylantracene. The reactions were carried out at reflux in the presence of CuI as co-catalyst in toluene/triethylamine as solvent. Due to the fast polymerization rate, the reactions had to be stopped after a few minutes, in order to avoid the formation of insoluble materials notwithstanding the presence of the *n*-octyl chains. Confirmation of the polymer structure was obtained by ^1H NMR, FTIR, as well as by elemental analyses. The number-average molecular weights (M_n) and PDIs of the synthesized polymers were evaluated by GPC. The thiophene-containing polymers **DBSTA** and **DTSTA** showed lower molecular weights ($M_n = 7400$ and 5600 Da, respectively) compared to the corresponding polymers **DBSA** and **DTSA** ($M_n = 16,200$ and 10,800 Da, respectively). This can be due to the lower solubility of **DBSTA** and **DTSTA** in the reaction medium, induced by the presence of the thiophene units, hampering the chain growth.

TGA revealed a satisfactory thermal stability of the synthesized polymers, as shown in Figure 1. The 5% weight loss decomposition temperatures for the dibenzosilole-containing polymers **DBSA** and **DBSTA** are lower (389 and 357 °C, respectively) compared to those obtained for the



SCHEME 2 Synthesis of the polymers. Reaction conditions: $\text{Pd}(\text{PPh}_3)_4/\text{CuI}$ in toluene triethylamine ($R = n\text{-octyl}$). Reaction conditions: $\text{Pd}(\text{PPh}_3)_4$, CuI , NEt_3 , toluene, reflux.

dithienosilole-containing **DTSA** and **DTSTA** (422 and 427 °C, respectively).

Optical Properties

The UV-vis spectra of **DTSA**, **DTSTA**, **DBSA**, and **DBSTA** were measured both in diluted chloroform solution (to rule out aggregation effects on the optical properties) and in the solid state (Figs. 2 and 3, respectively) by depositing them as thin films on quartz substrates. The UV-vis spectra of **DBSA** and **DBSTA** in chloroform solution show absorption maxima (λ_{max}) at 508 and 499 nm, respectively. The absorption profiles of **DBSA** and **DBSTA** in the solid state are slightly broadened and sensibly red-shifted with respect to those recorded in solution, exhibiting λ_{max} at 518 and 558 nm, respectively. The UV-vis spectra of **DTSA** show an

absorption peak that, in chloroform solution, is located at 562 nm while in the solid state it is red-shifted up to 601 nm. The absorption spectra of **DTSTA** shows a maximum at 545 nm in chloroform which is shifted to 586 nm in the solid state. The bathochromic shifts of the absorption profiles of all the four polymers as thin films can evidently be attributed to the enhanced intermolecular interactions occurring in solid state.

The introduction of thiophene bridges between the diethynyl-anthracene and the dibenzosilole units leads to the increase of the π -conjugation extension of **DBSTA** with respect to **DBSA** as evidenced by the observed decrease in optical band gap (E_g^{opt} , Table 1) measured both in solution and in the solid state. Counterintuitively, the optical

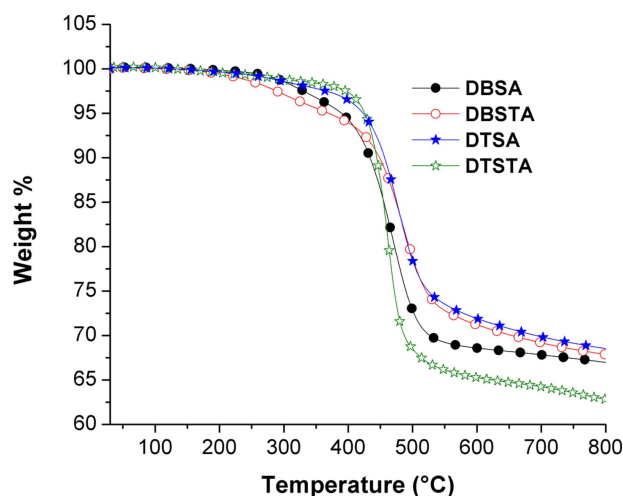


FIGURE 1 TGA plots obtained for the polymers. [Color figure can be viewed in the online issue, which is available at wileyonlinelibrary.com.]

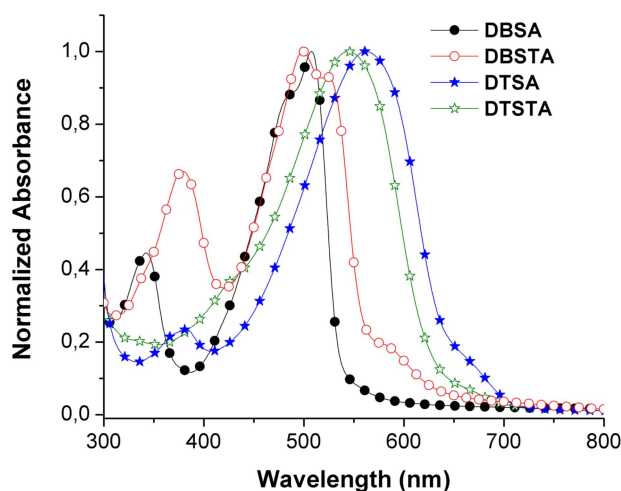


FIGURE 2 UV-vis spectra of the polymers in chloroform. [Color figure can be viewed in the online issue, which is available at wileyonlinelibrary.com.]

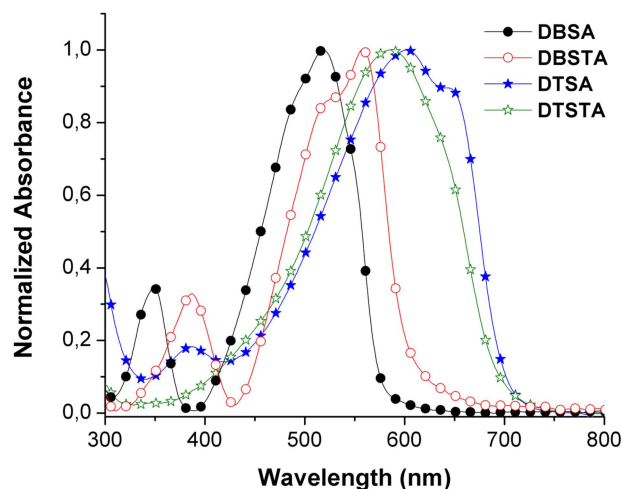


FIGURE 3 UV-vis spectra of the polymers as thin films. [Color figure can be viewed in the online issue, which is available at wileyonlinelibrary.com.]

properties of **DTSA** compared to those of **DTSTA** hint that the introduction of the thiophene units lead to a lowering of the π -conjugation extension. This behavior suggests that, in these poly(arylene-ethynylene)s, the degree of π -conjugation is influenced by the aromatic units chosen as well as by the π -conjugated backbone distortion. This aspect has been investigated (*vide infra*) by suitable theoretical calculations.

The presence of the thiophene units in **DTSTA** and **DBSTA** also strongly influences the molar absorption coefficients (ϵ) of the polymers, which were calculated in chloroform solutions by considering the M_n as its molecular weight.¹⁷ A very high ϵ_{\max} could be observed for **DBSA** and **DTSA** ($2.4 \times 10^6 \text{ M}^{-1}\text{cm}^{-1}$ and $8.6 \times 10^5 \text{ M}^{-1}\text{cm}^{-1}$, respectively) while the molar absorptivity is remarkably lower in the case of **DBSTA** and **DTSTA** ($\epsilon_{\max} = 1.4 \times 10^5 \text{ M}^{-1}\text{cm}^{-1}$ and $1.1 \times 10^5 \text{ M}^{-1}\text{cm}^{-1}$, respectively). This aspect determines the amount of photons absorbed by the active layer in a BHJ solar cell, which is higher in the case of **DBSA** and **DTSA** with respect to **DBSTA** and **DTSTA** thereby potentially influencing the photocurrent generation.

The PL spectra of the four copolymers in chloroform solutions were recorded and are shown in Figure 4. As reported in Table 1, the emission maxima (λ_{em}) followed the same trend of the optical band gaps, thus confirming the effects of

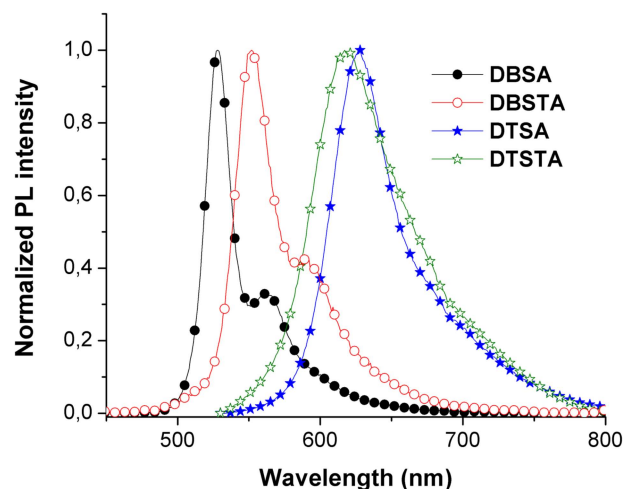


FIGURE 4 Normalized emission spectra of the polymers in chloroform. [Color figure can be viewed in the online issue, which is available at wileyonlinelibrary.com.]

the introduction of the thiophene units on the optical properties of the materials. While **DBSA** and **DBSTA** exhibited a vibronically structured emission profile, **DTSA** and **DTSTA** emitted with a broad PL band at longer wavelengths. Furthermore, the relatively low Stokes shifts observed (ranging from 745 to 2278 cm^{-1}) suggest the absence of an intramolecular charge transfer upon excitation, as a consequence of the electron-rich character of the aromatic units constituting the primary structures of the polymers. No PL spectra could be recorded for the copolymers as thin films, suggesting the occurrence of strong intermolecular interactions in the solid state. It is plausible that the intermolecular π - π stacking, probably favored by the anthracene units, leads to radiative deactivation pathways of the polymer excited states, with the consequent quenching of their emission.

Electrochemical Properties

CV measurements allowed the assessment of the HOMO and LUMO energy levels of the synthesized polymers. Representative CV curves are shown in Figure 5, while the obtained HOMO and LUMO values are reported in Table 1. The cyclic voltammograms of both **DTSA** and **DTSTA** showed quasi-reversible p-doping (oxidation/re-reduction) and quasi-reversible n-doping (reduction/reoxidation) processes. A similar CV behavior was observed for **DBSTA**, while **DBSA**

TABLE 1 Optical and Electrochemical Properties of **DTSA**, **DTSTA**, **DBSA**, and **DBSTA**: UV-Vis and PL Data Obtained Both in Chloroform and in the Solid State; HOMO and LUMO Energies Obtained From Cyclic Voltammetry

	$\lambda_{\max \text{ sol}}$ (nm)	$\lambda_{\max \text{ film}}$ (nm)	$E_g^{\text{opt sol}}$ (eV)	$E_g^{\text{opt film}}$ (eV)	$\lambda_{\text{em sol}}$ (nm)	HOMO (eV)	LUMO (eV)	E_g^{elc} (eV)
DBSA	508	518	2.31	2.16	528	-5.6	-3.3	2.3
DBSTA	499	558	2.19	2.06	552	-5.4	-3.3	2.1
DTSA	562	602	1.87	1.74	627	-5.2	-3.4	1.8
DTSTA	544	586	1.93	1.80	621	-5.3	-3.4	1.9

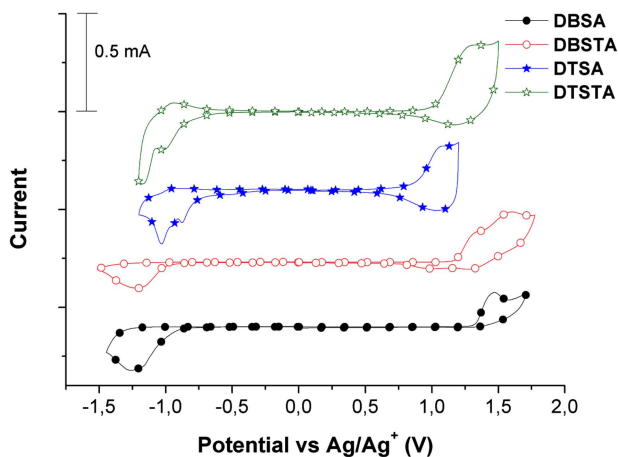


FIGURE 5 CV traces of the synthesized polymers. [Color figure can be viewed in the online issue, which is available at wileyonlinelibrary.com.]

exhibited both anodic and cathodic irreversible events.¹⁸ Concerning the HOMO and LUMO energy levels and the electrochemical energy gap (E_g^{elc}), the incorporation of the thiophene spacers led to a substantial HOMO-level increase passing from -5.6 eV for **DBSA** to -5.4 eV for **DBSTA**, while the LUMO energy levels of both polymers are the same (-3.3 eV). As a result, the observed E_g^{elc} of **DBSTA** (2.1 eV) is lower than that of **DTSA** (2.3 eV).

On the contrary, the insertion of the thiophene units in **DTSTA** induced a lowering of the HOMO energy value (-5.3 eV) compared to that of **DTSA** (-5.2 eV). Again, no effects could be observed on the LUMO energy levels (-3.4 eV for both polymers) and consequently the observed E_g^{elc} of **DTSTA** (1.9 eV) results higher than that of **DTSA** (1.8 eV). The trend observed for the E_g^{elc} , therefore, follows the one previously discussed for the E_g^{opt} . From the analysis of the aforementioned results, it can be concluded that the synthesized polymers hold the suitable requisites to efficiently operate, at least in principle, within a BHJ solar cell: their HOMO energy levels are in fact favorably aligned with the ITO workfunction (-4.7 eV) and their LUMO energy levels are compatible with an efficient photoreduction of the common fullerene-based electron-acceptors (endowed with a LUMO of ~ -4.3 eV) used in the donor-acceptor blend constituting the photoactive layer. It appears, however, that **DTSA** and **DTSTA** hold better features in terms of light harvesting properties: their band gap is in fact remarkably lower with respect to that of **DBSA** and **DBSTA**.

Theoretical Calculations

Theoretical methods are helpful for gaining insight into the electronic structure as well as into the optical properties of conjugated materials. It must be noted however that, for polymers, several parameters such as the molecular orbital energies and the excitation vertical transitions, are strongly influenced by the number of the repeating units of the model chosen for the calculation. Therefore, in order to draw reliable conclusions from the theoretical results obtained for a

given primary structure, the calculations should be carried out on appropriate finite models, of increasing size, and then by extrapolating the chosen parameters for an hypothetically infinite polymer segment. To this purpose, DFT and TDDFT calculations were carried out on the repeating unit (monomer) of each polymer as well as on oligomers, from dimers to tetramers ($n = 1-4$ in Scheme 2).

It can be assumed that the length of the alkyl chains at the bridging silicon atom of the dibenzosilole and dithienosilole units do not exert a significant influence on the geometry of the selected polymer segments. On this ground, the *n*-octyl chains were replaced by $-\text{CH}_3$ groups, in order to reduce the computational load. Geometry optimization was performed *in vacuo* and carried out using the B3LYP functional with the 3-21G(d) basis set, also allowing the description of extended systems containing a large number of atoms. Subsequently, starting from the optimized geometries obtained, the HOMO and LUMO energy values were determined for each model structure using the 6-31G(d,p) basis set. The TDDFT calculations were carried out using the CAM-B3LYP functional and the 3-21G(d) basis set.

Plotting the HOMO, LUMO, and the lowest excitation energies of the oligomers against $1/n$ (where n indicates the number of repeating units of the selected models), it is possible to extrapolate the values ideally obtainable for a polymer segment of virtually infinite length, as the intercept with the ordinate axes, using a linear fit.¹⁹ This approach becomes mandatory for an accurate comparison between polymers constituted by repeating units containing a different amount of aromatic units, such as **DTSTA** (**DBSTA**) compared to **DTSA** (**DBSA**).

The relevant results are shown in Figures 6 and 7 and are summarized in Table 2. Concerning the HOMO and LUMO energy values extrapolated for $1/n = 0$, these are in excellent

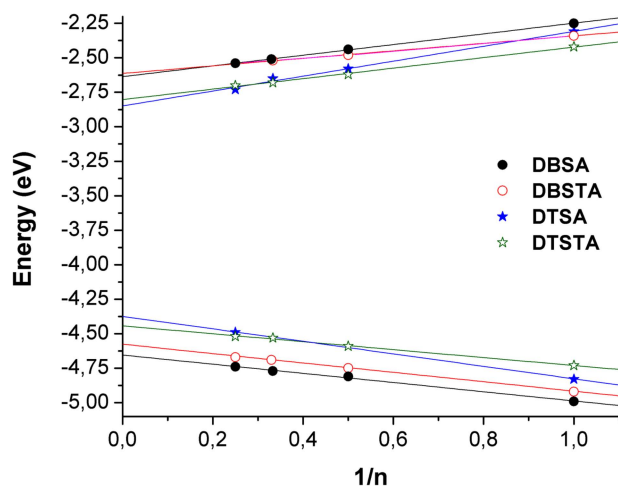


FIGURE 6 Calculated linear trends ($R > 0.99$) of HOMO and LUMO energy values for the model structures ($n = 1-4$) of the synthesized polymers. [Color figure can be viewed in the online issue, which is available at wileyonlinelibrary.com.]

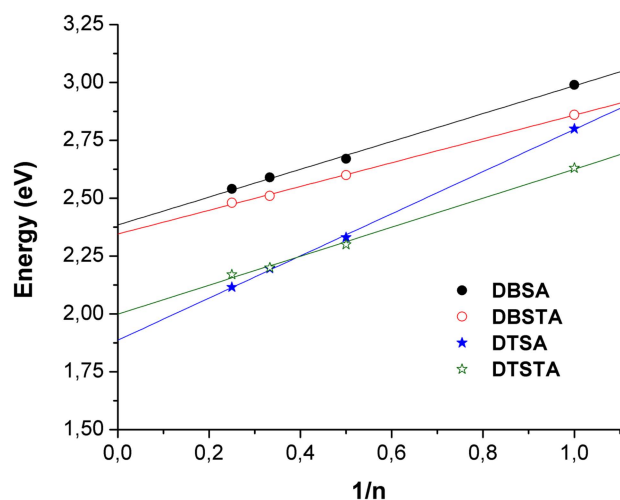


FIGURE 7 Calculated linear trends ($R > 0.99$) of the lowest excitation energies for the model structures ($n = 1-4$) of the synthesized polymers. [Color figure can be viewed in the online issue, which is available at www.interscience.wiley.com.]

agreement with the experimental estimates of optical and electrochemical band gaps. Also in the case of the excitation energies, the extrapolated values are in good agreement with the found optical band gaps measured for diluted solutions, as shown in Figure 7. Remarkably, DFT and TDDFT calculations confirm that the incorporation of the thienylene units leads to different effects in dibenzosilole- and dithienosilole-containing polymers, in particular, the higher extrapolated excitation energy calculated for the **DTSTA** model justifies the counterintuitive blue-shifted absorption of **DTSTA** with respect to **DTSA** (*vide supra*) observed in the UV-vis spectra. It is very likely that the explanation of this peculiar behavior may reside in the distortion of the copolymer backbone, that, limiting the conjugation extension, counterbalances the band gap contraction promoted by the incorporation of the low-energy thiophene units.

In fact, as illustrated in Figure 8, the **DBSA** and **DTSA** models show an extremely planar structure, since the torsion angle between the silole and anthracene planes in relatively long segments (trimers) lies between 0.46° and 4.77° , due to the presence of the ethynylene spacers between the aryl moieties. In the case of **DBSTA** and **DTSTA**, conversely, the dihedral angles between the silole and thiophene units are higher and comprised between 23° and 26° , while the remaining part of the conjugated segment lies close to planarity.

The calculated electron density distributions of the HOMO and LUMO levels along with the optimized geometry obtained for selected segments (trimers) of the polymers are shown in Figure 8. It can be stated that the HOMOs of the polymers are evenly distributed along the entire chain, hinting a good hole transport ability (at least along the conjugated backbone) after the electron transfer to the fullerene acceptor in a BHJ solar cell. Differently from the polymeric

structures characterized by an intramolecular charge transfer, also the LUMOs are evenly distributed along the entire chain. Furthermore, according to the TDDFT results, the main transition ($S_0 \rightarrow S_1$) of the selected segments of the polymers is predominantly described by a HOMO \rightarrow LUMO transition.

Photovoltaic Characterization

The photovoltaic properties of the synthesized polymers were investigated in BHJ solar cells of configuration: ITO/PEDOT:PSS/polymer:PC₆₁BM/LiF/Al. We tested the polymers in different donor:acceptor ratios. As reported in Table 3, the best figures of merit in terms of power conversion efficiency (PCE) for each material were obtained using a polymer:PC₆₁BM blend ratio of 40:60. Figure 9 shows the characteristic current density–voltage ($J-V$) plots obtained for the best devices. In particular, the best performing devices were obtained with **DTSA** and afforded a PCE of 1.50%; the short circuit current density (J_{sc}), open circuit voltage (V_{oc}), and fill factor (FF) were 5.97 mA cm^{-2} , 0.68 V, and 37%, respectively. The devices based on the analogous thiophene-containing polymer **DTSTA** were characterized by a decrease in all figures of merit, leading to a very poor (PCE = 0.20%) overall efficiency, substantially ascribable to the poor quality of the blend films caused by the limited solubility of the material. In the case of the dibenzosilole-based polymers **DBSA** and **DBSTA**, their poorer performances can be reasonably explained by their higher energy gap with respect to that of **DTSA**. Analyzing in detail their figures of merit, however, **DBSA** showed a less efficient photocurrent generation ($J_{sc} = 2.25 \text{ mA cm}^{-2}$) with respect to that of **DBSTA** ($J_{sc} = 3.76 \text{ mA cm}^{-2}$) probably ascribable to its slightly

TABLE 2 Calculated HOMO, LUMO, and Lowest Excitation Energies of **DBSA**, **DBSTA**, **DTSA**, and **DTSTA**

	HOMO ^a n (eV)	LUMO ^a (eV)	Exc. En. ^b (eV)	HOMO ^a (eV)	LUMO ^a (eV)	Exc. En. ^b (eV)
	DBSA			DBSTA		
1	-4.99	-2.25	2.98	-4.92	-2.34	2.86
2	-4.82	-2.44	2.67	-4.75	-2.49	2.60
3	-4.77	-2.51	2.59	-4.69	-2.52	2.51
4	-4.74	-2.54	2.54	-4.67	-2.54	2.47
fit	-4.65	-2.64	2.38	-4.58	-2.62	2.34
	DTSA			DTSTA		
1	-4.83	-2.29	2.79	-4.73	-2.43	2.62
2	-4.59	-2.57	2.34	-4.60	-2.63	2.30
3	-4.53	-2.64	2.20	-4.54	-2.69	2.20
4	-4.48	-2.74	2.11	-4.52	-2.70	2.16
fit	-4.38	-2.86	1.89	-4.45	-2.81	2.00

^aCalculated at the B3LYP/6-31G(d,p) level based on B3LYP/3-21G(d) optimized geometries.

^bTDDFT excitation energies calculated on the B3LYP/3-21G(d) optimized geometries with the CAM-B3LYP functional using the 3-21G(d) basis set.

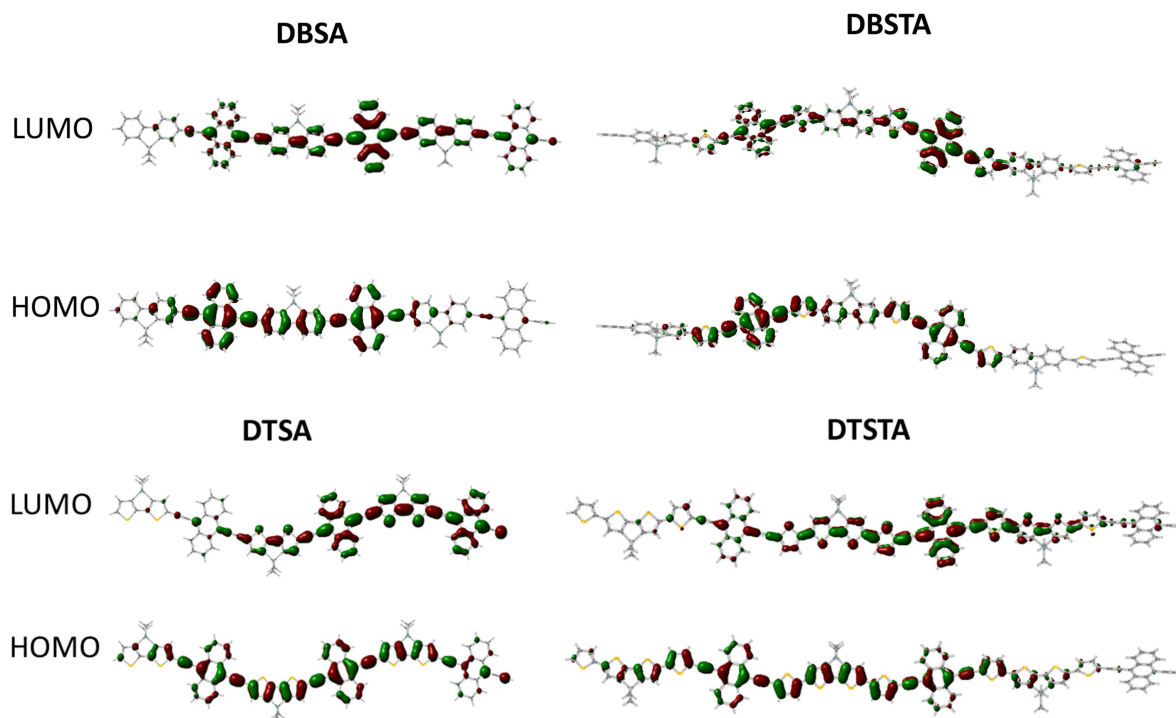


FIGURE 8 Isodensity (0.02) plots of HOMOs and LUMOs for the trimers ($n=3$) of **DBSA**, **DBSTA**, **DTSA**, and **DTSTA**. [Color figure can be viewed in the online issue, which is available at wileyonlinelibrary.com.]

narrower and blue shifted (see Fig. 3) absorption profile. Conversely, due to its lower HOMO energy value, **DBSA** devices exhibited a remarkably higher V_{OC} with respect to **DBSTA**-based ones (0.75 V respect to 0.49 V for the best devices).

It is known that the variation of the polymer/ $PC_{61}BM$ blend ratios significantly affects the photovoltaic response of the BHJ solar cell. A slight increase (70% respect to the poly-

mer) of the $PC_{61}BM$ amount in the blend ratio (Table 3) led to lower performances in terms of PCE recorded for each polymer. This behavior might be ascribable to a less efficient charge transport deriving from an unfavorable organization of the interpenetrating network between the polymer and $PC_{61}BM$ phases. However, the same PCE response was observed by increasing the polymer amount in the blend films (up to 60% wt/wt), notwithstanding the plausible higher efficiency in the light harvesting process. This result confirms that the optimal tridimensional organization of the polymer/ $PC_{61}BM$ phases exerts a key role in the performances exhibited by these polymers.

TABLE 3 Photovoltaic Parameters Obtained for the BHJ Devices of Configuration ITO/PEDOT-PSS/Polymer: $PC_{61}BM$ /LiF/Al

	Polymer: $PC_{61}BM$ Ratio (wt:wt)	PCE (%)	FF (%)	V_{OC} (V)	J_{SC} ($mA\ cm^{-2}$)
DBSA	30:70	0.42	28	0.71	2.15
	40:60	0.52	31	0.75	2.25
	60:40	0.20	28	0.75	0.95
DBSTA	30:70	0.42	31	0.43	3.13
	40:60	0.59	32	0.49	3.76
	60:40	0.35	30	0.40	2.88
DTSA	30:70	0.52	36	0.49	2.98
	40:60	1.50	37	0.68	5.97
	60:40	0.55	29	0.39	4.85
DTSTA	30:70	0.12	28	0.23	1.83
	40:60	0.20	22	0.55	1.62
	60:40	0.19	29	0.32	2.03

A fundamental property to be evaluated for a polymeric donor material is its hole mobility, since the charge transport can also influence the performance of a BHJ device. In order to tackle this issue, suitable top-contact organic field-effect transistors (OFET) were constructed and their transfer characteristics were measured. As expected, a p-type behavior for each transistor was observed. Except for **DBSA**, that did not exhibit modulation, average extracted hole mobilities were $1.50 \times 10^{-4}\ cm^2\ V^{-1}\ s^{-1}$ (**DBSTA**), $3.50 \times 10^{-5}\ cm^2\ V^{-1}\ s^{-1}$ (**DTSA**) and $6.80 \times 10^{-5}\ cm^2\ V^{-1}\ s^{-1}$ (**DTSTA**). The obtained hole mobilities are in line with those exhibited by other polymers showing similar photovoltaic performances.²⁰ The transfer curves of the materials (see Supporting Information) showed a remarkably higher average threshold voltage (V_{th}) for the dibenzosilole-containing polymer (-29 V for **DBSTA**) indicating a relatively high density of charge carrier traps for this material with respect to **DTSTA** and

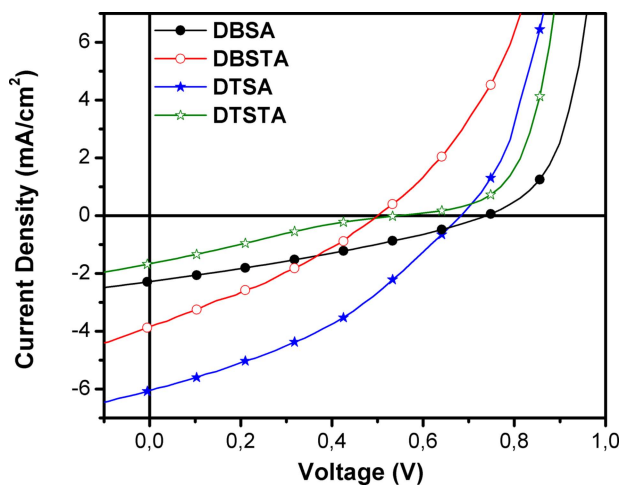


FIGURE 9 J - V plots obtained for the devices of configuration ITO/PEDOT-PSS/polymer:PC₆₁BM/LiF/Al at a polymer:PC₆₁BM blend ratio of 40:60 (wt/wt). [Color figure can be viewed in the online issue, which is available at wileyonlinelibrary.com.]

DTSA, showing V_{th} of -4 and -18 V, respectively. The on/off ratios ($\sim 10^2$) were very similar for all the polymers. From these results, it is apparent that the introduction of the thiophene units in **DBSTA** and **DTSTA** substantially increases the hole mobility with respect to their counterparts **DBSA** and **DTSA**. This observation can be explicable by admitting a higher degree of π - π interactions between adjacent conjugated backbones, as is usually observed for organic semiconductors for OFET.²¹ However, especially comparing the field-effect transistor and the BHJ solar cell performances obtained for **DTSTA** with respect to **DTSA**, the increased hole mobility of **DTSTA** did not lead to a consequent improvement in photovoltaic response. It is reasonable to suppose that, despite the favorable absorption profile and hole mobility recorded in OFET, the reasons for the poor BHJ solar cell figures of merit of **DTSTA** are solely to be searched in the formation of a nonsuitable polymer/PC₆₁BM interface with a consequent negative influence on the charge photogeneration.

To this purpose, knowing that nanoscale phase separation of the photoactive layer on the performance of OPVs is a critical issue, and in order to corroborate the observations on the electronic and photovoltaic properties of the new materials with information on the mesoscopic characterization of the blends, tapping mode AFM measurements (see Supporting Information Figs. S8–S11) were carried out on the 40:60 wt/wt polymer:PC₆₁BM blend film that gave the best results in terms of PCE. While the **DBSA**-, **DBSTA**-, and **DTSA**-based blend films revealed similar morphologies, it was observed that the **DTSTA**:PC₆₁BM film revealed bigger domain sizes. It seems rational to assume that the higher tendency toward interchain interaction of **DTSTA**, hinted by its higher field-effect mobility, can also be held responsible for the segregation of the polymer/PC₆₁BM phases which results detrimental in terms of its photovoltaic efficiency.

Photochemical Stability

In order to qualify a suitably designed π -conjugated polymer (which is the main responsible for the light-harvesting) as promising donor for BHJ solar cells, the photoconversion efficiency value reached by the material in the devices has to be accompanied by a marked optical stability under the operating conditions. Changes in the absorption profile and intensity of the polymer donor can, in fact, lead to a degradation of the PCE of the device, deriving from a decreased amount of absorbed photons by the active layer. The chemical nature of polyconjugated materials specifically designed as light harvesters in organic photovoltaics makes them vulnerable toward photo-oxidation.²² Although photovoltaic devices can be efficiently protected from the atmosphere by encapsulation, oxygen traces can, in the course of the device lifetime, come in contact with the photoactive organic film, triggering well-established radicalic pathways for organic semiconductors²³ rapidly leading to deterioration of the performances. On the basis of the aforementioned considerations, accelerated degradation tests carried out under ambient conditions can provide a wealth of data on the photostability of a donor material for BHJ solar cells considerably reducing investigation times on these issues.

In setting up a photo-degradation accelerated test, it should be taken into account that the visible portion (400–700 nm) of the sun-light is partially absorbed by the polymer donor, giving rise to an excited state the lifetime of which is in the subnanoseconds range, due to the very fast electron transfer to the fullerene acceptor.²⁴ As a consequence, polymer degradation is not likely to occur while the polymer is in its excited state. Conversely, specific degradation pathways leading to undesired variations in the absorption spectrum of the polymer donor can be triggered by the high-energy photons in the UV portion ($\sim 5\%$) of the solar spectrum.²⁵

For these reasons, it was chosen to study the photochemical stability of **DTSA** (the material showing the best figures of

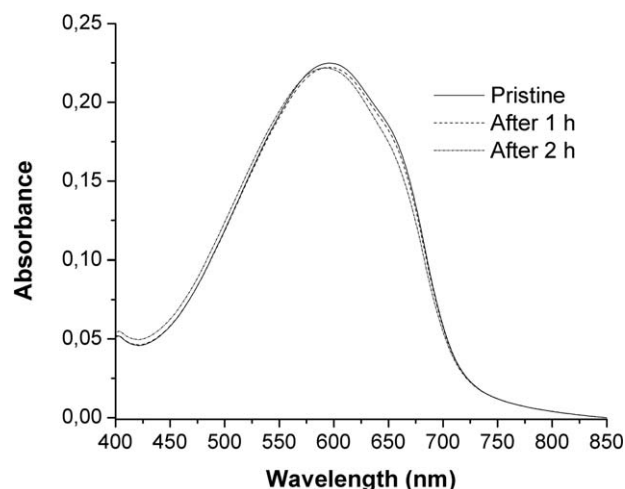


FIGURE 10 Evolution of the UV-visible spectrum of **DTSA** as thin films during UV-promoted photo-oxidation.

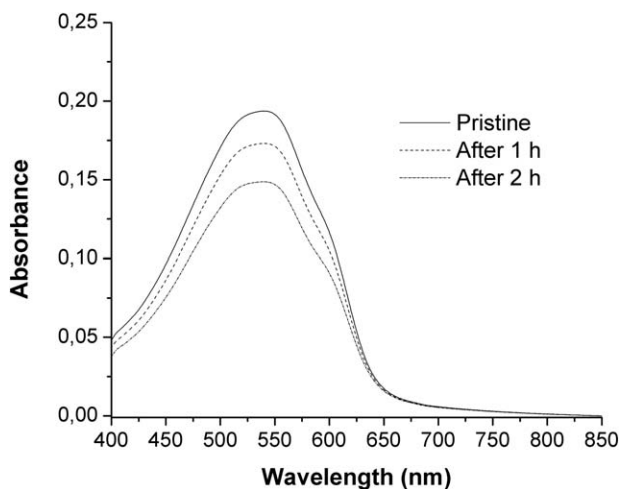


FIGURE 11 Evolution of the UV-visible spectrum of P3HT as thin films during UV-promoted photo-oxidation.

merit in BHJ devices) by illuminating a spin-coated film of the polymer with a UV lamp in air. As shown in Figure 10, the photo-oxidation treatment did not induce substantial changes in the absorbance of **DTSA**, while the observed slight variations in the absorption profile could be attributed to the polymer chains rearrangements, probably due to the increase of the temperature during the irradiation.

In order to confirm the photostability of **DTSA**, the same experiment was carried out on a film of poly(3-hexyl)thiophene (P3HT), which is the prototypical all-donor material for BHJ solar cells due to its efficiencies in devices. For the P3HT film, a continuous decrease in the intensity of the absorption band accompanied by a slight blue-shift of the absorption maximum was observed (Fig. 11) during the irradiation. It is widely accepted that the degradation of P3HT involves the radical oxidation of the alkyl side chains with the subsequent stepwise oxidation of the sulfur atom of the thiophene rings.²⁶ The consequent cleavage of the polymer backbone results in a loss of π -conjugation, leading to a lowering of the absorbance. The optical instability of P3HT is due to the loss of the hydrogen atom belonging to the α -methylene group of the alkyl chain with the formation of a benzylic-type radical with high mesomeric stability, which can be considered the “trigger” of the material degradation. The propagation of the radicalic degradation is not only suggested by the aforementioned modifications of the absorption spectrum, but is also corroborated by the fact that, after exposure to the UV irradiation, the resulting material is insoluble in chloroform, which can be a consequence of a radical promoted crosslinking between adjacent polymer chains.

Conversely, in the case of **DTSA**, the film recovered after the UV exposure was almost completely soluble in chloroform, suggesting that the radical promoted degradation was inhibited for this material. This aspect can be rationalized in view of the fact that the formation of mesomerically stabilized

radicals in **DTSA** is ruled out by the presence of the quaternary silicon atom,²⁷ which is much less prone to oxidation with respect to the α -methylene group of the *n*-hexyl chains in P3HT. Furthermore, the photochemical stability of **DTSA** is reinforced by the 9,10-diethynyl-anthracene units, the presence of which, as also observed for other polycyclic aromatic units,²⁸ seems to inhibit the photo-induced degradation of the corresponding polymers.

CONCLUSIONS

Instead of the mere search for the highest performances obtainable by light-harvesting materials in BHJ solar cells, the evaluation of the structure-property relationships between polymers belonging to a specific class of organic semiconductors is a valuable tool in order to conceive new donor architectures for organic photovoltaics. To this purpose, four new all-donor copolymers containing silole-based units (i.e., dibenzosilole, dithienyl-dibenzosilole, dithienosilole or dithienyl-dithienosilole) and 9,10-diethynyl-anthracene units were synthesized by Sonogashira polycondensation reactions. These alternating poly(arylene-ethynylenes) were characterized by NMR, IR, UV-vis, PL, and CV. The dithienosilole- and dithienyl-dithienosilole-based polymers (**DTSA** and **DTSTA**) were identified as plausible candidates for BHJ applications due to their light-harvesting properties, and this choice was corroborated by DFT calculations carried out on suitable finite model systems of the four polymeric architectures. As a matter of fact, in BHJ devices **DBSA** and **DBSTA** did not exceed a PCE of 0.59%. Conversely, despite a higher field-effect hole mobility exhibited by **DTSTA** with respect to its thiophene-free counterpart **DTSA**, organic BHJ solar cells embodying PC₆₁BM as electron acceptors revealed that **DTSA** is extremely more performing with respect to **DTSTA** (PCE 0.20%) probably due to the formation of an unsuitable blend between **DTSTA** and the acceptor, caused by strong intermolecular interactions between adjacent polymer chains, as suggested by AFM investigations. Remarkably, the PCE value (1.50%) obtained with **DTSA** represents one of the highest efficiencies obtained for BHJ solar cells based on all-donor polymers constructed without the use of additives or of annealing processes. Last but not least, UV-promoted degradation of **DTSA** films under air evidenced a remarkable photostability of this material with respect to the well-known P3HT donor. Further improvements can be expected by an optimization of the processing conditions as well as by increasing of the molecular weights and solubility for this class of new organic semiconductors.

ACKNOWLEDGMENTS

The authors gratefully acknowledge for funding: Regione Puglia (APQ-Reti di Laboratorio, Project PHOEBUS, cod. 31-FE1. 20001); MIUR (PRIN 2009 project 2009AZKNJ7); MAAT-Molecular Nanotechnology for Health and Environment (PON02_00563_3316357); EFOR-Energia da Fonti Rinnovabili (Iniziativa CNR per il Mezzogiorno L. 191/2009 art. 2 comma 44).

REFERENCES AND NOTES

- 1 (a) P.-L. Boudreault, T. A. Najari, M. Leclerc, *Chem. Mater.* **2011**, *23*, 456–469; (b) M. Helgesen, R. Søndergaard, F. C. Krebs, *J. Mater. Chem.* **2010**, *20*, 36–60; (c) S. Günes, H. Neugebauer, N. S. Sariciftci, *Chem. Rev.* **2007**, *107*, 1324–1338.
- 2 (a) H. Zhou, L. Yang, W. You, *Macromolecules* **2012**, *45*, 607–632; (b) C. J. Brabec, S. Gowrisanker, J. J. M. Halls, D. Laird, S. Jia, S. P. Williams, *Adv. Mater.* **2010**, *22*, 3839–3856; (c) R. Lecover, N. Williams, N. Markovic, D. H. Reich, D. O. Naiman, H. E. Katz, *ACS Nano* **2012**, *6*, 2865–2870.
- 3 (a) N. Blouin, M. Leclerc, *Acc. Chem. Res.* **2008**, *41*, 1110–1119; (b) H. A. M. van Mullekom, J. A. J. M. Vekemans, E. E. Havinga, E. W. Meijer, *Mater. Sci. Eng. R* **2001**, *32*, 1–40; (c) E. E. Havinga, W. Hove, H. Wynberg, *Synth. Met.* **1993**, *229*, 55–57.
- 4 See for example: G. Li, V. Shrotriya, J. Huang, Y. Yao, T. Moriarty, K. Emery, Y. Yang, *Nat. Mater.* **2005**, *4*, 864–868.
- 5 P. M. Beaujuge, W. Pisula, H. N. Tsao, S. Ellinger, K. Müllen, J. R. Reynolds, *J. Am. Chem. Soc.* **2009**, *131*, 7514–7515.
- 6 (a) R. S. Ashraf, J. Gilot, R. A. J. Janssen, *Sol. Energy Mater. Sol. Cells* **2010**, *94*, 1759–1766; (b) R. S. Ashraf, M. Shahid, E. Klemm, M. Al-Ibrahim, S. Sensfuss, *Macromol. Rapid Commun.* **2006**, *27*, 1454–1459.
- 7 J.E. Anthony, *Chem. Rev.* **2006**, *106*, 5028–5048.
- 8 (a) M. Seri, A. Marrocchi, D. Bagnis, R. Ponce, A. Taticchi, T. J. Marks, A. Facchetti, *Adv. Mater.* **2011**, *23*, 3827–3831; (b) D. K. Susarova, E. A. Khakina, P. A. Troshin, A. E. Goryachev, N. S. Sariciftci, V. F. Razumov, D. A. M. Egbe, *J. Mater. Chem.* **2011**, *21*, 2356–2361; (c) F. Silvestri, A. Marrocchi, M. Seri, C. Kim, T. J. Marks, A. Facchetti, A. Taticchi, *J. Am. Chem. Soc.* **2010**, *132*, 6108–6123; (d) A. Marrocchi, F. Silvestri, M. Seri, A. Facchetti, A. Taticchi, T. J. Marks, *Chem. Commun.* **2009**, 1380–1382.
- 9 (a) S. Rathbeger, J. Perlich, F. Kühnlenz, S. Türk, D. A. M. Egbe, H. Hoppe, R. Gehrke, *Polymer* **2011**, *52*, 3819–3826; (b) D. A. M. Egbe, S. Türk, S. Rathbeger, F. Kühnlenz, R. Jadhav, A. Wild, E. Birkner, G. Adam, A. Pivrikas, V. Cimrova, G. Knör, N. S. Sariciftci, H. Hoppe, *Macromolecules* **2010**, *43*, 1261–1269; (c) S. Rathbeger, D. B. de Toledo, E. Birkner, H. Hoppe, D. A. M. Egbe, *Macromolecules* **2010**, *43*, 306–315; (d) S. Günes, A. Wild, E. Cevik, A. Pivrikas, U. S. Schubert, D. M. Egbe, *Sol. Energy Mater. Sol. Cells* **2010**, *94*, 484–491.
- 10 S. Yamaguchi, K. Tamao, *J. Chem. Soc. Dalton Trans.* **1998**, 3693–3702.
- 11 (a) M. C. Scharber, M. Koppe, J. Gao, F. Cordella, M. A. Loi, P. Denk, M. Morana, H.-J. Egelhaaf, K. Forberich, G. Dennler, R. Gaudiana, D. Waller, Z. Zhu, X. Shi, C. J. Brabec, *Adv. Mater.* **2010**, *22*, 367–370; (b) J. Ding, N. Song, Z. Li, *Chem. Commun.* **2010**, *46*, 8668–8670; (c) J. Ohshita, *Macromol. Chem. Phys.* **2009**, *210*, 1360–1370; (d) L. Huo, H.-Y. Chen, J. Hou, T. L. Chen, Y. Yang, *Chem. Commun.* **2009**, 5570–5572; (e) J. Hou, H.-Y. Chen, S. Zhang, G. Li, Y. Yang, *J. Am. Chem. Soc.* **2008**, *130*, 16144–16145; (f) J. Chen, Y. Cao, *Macromol. Rapid Commun.* **2007**, *28*, 1714–1742; (g) L. Liao, L. Dai, A. Smith, M. Durstock, J. Lu, J. Ding, Y. Tao, *Macromolecules* **2007**, *40*, 9406–9412; (h) H. Usta, G. Lu, A. Facchetti, T. J. Marks, *J. Am. Chem. Soc.* **2006**, *128*, 9034–9035.
- 12 (a) R. Grisorio, G. Allegretta, G. P. Suranna, P. Mastorilli, A. Loiudice, A. Rizzo, M. Mazzeo, G. Gigli, *J. Mater. Chem.* **2012**, *22*, 19752–19760; (b) G. Romanazzi, A. Dell’Aquila, G. P. Suranna, F. Marinelli, S. Cotrone, D. Altamura, C. Giannini, L. Torsi, P. Mastorilli, *J. Mater. Chem.* **2011**, *21*, 15186–15189.
- 13 S. Colella, M. Mazzeo, R. Grisorio, E. Fabiano, G. Melcarne, S. Carallo, M. D. Angione, L. Torsi, G. P. Suranna, F. della Sala, P. Mastorilli, G. Gigli, *Chem. Commun.* **2010**, 6273–6275.
- 14 K. L. Chan, M. J. McKiernan, C. R. Towns, A. B. Holmes, *J. Am. Chem. Soc.* **2005**, *127*, 7662–7663.
- 15 D. R. Coulson, L. C. Satek, S. O. Grim, *Inorg. Synth.* **1972**, *13*, 121–124.
- 16 M. J. Frisch, G. W. Trucks, H. B. Schlegel, G. E. Scuseria, M. A. Robb, J. R. Cheeseman, G. Scalmani, V. Barone, B. Menonucci, G. A. Petersson, H. Nakatsuji, M. Caricato, X. Li, H. P. Hratchian, A. F. Izmaylov, J. Bloino, G. Zheng, J. L. Sonnenberg, M. Hada, M. Ehara, K. Toyota, R. Fukuda, J. Hasegawa, M. Ishida, T. Nakajima, Y. Honda, O. Kitao, H. Nakai, T. Vreven, J. A. Montgomery, Jr., J. E. Peralta, F. Ogliaro, M. Bearpark, J. J. Heyd, E. Brothers, K. N. Kudin, V. N. Staroverov, R. Kobayashi, J. Normand, K. Raghavachari, A. Rendell, J. C. Burant, S. S. Iyengar, J. Tomasi, M. Cossi, N. Rega, J. M. Millam, M. Klene, J. E. Knox, J. B. Cross, V. Bakken, C. Adamo, J. Jaramillo, R. Gomperts, R. E. Stratmann, O. Yazyev, A. J. Austin, R. Cammi, C. Pomelli, J. W. Ochterski, R. L. Martin, K. Morokuma, V. G. Zakrzewski, G. A. Voth, P. Salvador, J. J. Dannenberg, S. Dapprich, A. D. Daniels, Ö. Farkas, J. B. Foresman, J. V. Ortiz, J. Cioslowski, and D. J. Fox, Gaussian, Inc., Wallingford CT, **2009**.
- 17 M. Coakley, M. D. McGehee, *Chem. Mater.* **2004**, *16*, 4533–4542.
- 18 E. Wang, C. Li, W. Zhuang, J. Peng, Y. Cao, *J. Mater. Chem.* **2008**, *18*, 797–801.
- 19 B. P. Karsten, J. C. Bijleveld, L. Viani, J. Cornil, J. Gierschner, R. A. J. Janssen, *J. Mater. Chem.* **2009**, *19*, 5343–5350.
- 20 See, for example: J. Kim, S. H. Kim, I. H. Jung, E. Jeong, Y. Xia, S. Cho, I.-W. Hwang, K. Lee, H. Suh, H.-K. Shim, H. Y. Woo, *J. Mater. Chem.* **2010**, *20*, 1577–1586.
- 21 C. Wang, H. Dong, W. Hu, Y. Liu, D. Zhu, *Chem. Rev.* **2012**, *112*, 2208–2267.
- 22 M. Jørgensen, K. Norrman, S. A. Gevorgyan, T. Tromholt, B. Andreasen, F. C. Krebs, *Adv. Mater.* **2012**, *24*, 580–612.
- 23 R. Grisorio, G. Allegretta, P. Mastorilli, G. P. Suranna, *Macromolecules* **2011**, *44*, 7977–7986.
- 24 C. J. Brabec, G. Zerza, G. Cerullo, S. De Silvestri, S. Luzzati, J. C. Hummelen, S. Sariciftci, *Chem. Phys. Lett.* **2001**, *340*, 232–236.
- 25 H. Hintz, H.-J. Egelhaaf, L. Lüer, J. Hauch, H. Peisert, T. Chasse, *Chem. Mater.* **2011**, *23*, 145–154.
- 26 M. Manceau, A. Rivaton, J.-L. Gardette, S. Guillerez, N. Lemaitre, *Polym. Degrad. Stab.* **2009**, *94*, 898–907.
- 27 M. Manceau, E. Bundgaard, J. E. Carlé, O. Hagemann, M. Helgesen, R. Søndergaard, M. Jørgensen, F. C. Krebs, *J. Mater. Chem.* **2011**, *21*, 4132–4141.
- 28 E. Bundgaard, O. Hagemann, M. Manceau, M. Jørgensen, F. C. Krebs, *Macromolecules* **2010**, *43*, 8115–8120.